Non-orographic gravity waves: representation in climate models and effects on infrasound

David Cugnet, A de La Camara, F. Lott, C Millet, B Ribstein

Non-orographic gravity waves: representation in climate models and effects on infrasound

D. Cugnet[1], A. de la Camara[2], F. Lott[1], C. Millet[3,4], and B. Ribstein[4,3]

[1]LMD, PSL Reasearch University, Ecole Normale Suprieure, Paris, France
[2]Dpto. Fsica de la Tierra y Astrofsica, Univ. Complutense de Madrid, Spain
[3]CEA, DAM, DIF, F-91297 Arpajon, France
[4]CMLA, ENS Cachan, CNRS, Université Paris-Saclay, 94235 Cachan, France

Corresponding author: François Lott, flott@lmd.ens.fr

Abstract

Long-range infrasound propagation is controlled by atmospheric waveguides that extend up to the mesosphere and lower thermosphere and whose efficiency is affected by gravity waves (GWs). These GWs are not explicitely represented in the global models often used to calculate infrasound propagation because their spatial scales are well below the models resolution. These unresolved GWs also transport momentum and control in good part the large-scale circulation in the middle atmosphere. These two issues make that the GWs need to be parameterized to improve the datasets used to calculate infrasound propagation as well as in the Atmospheric General Circulation Models (AGCMs) that are used to make weather forecasts and climate predictions. These two issues gain in being treated in conjonction. From this, improved infrasound calculations could be made by using a realistic amount of GWs. In return, using infrasound records could help specifying important characteristics of the GWs that are parameterized in the climate models.

The paper presents a research framework developed to address these issues. It first presents a non-orographic GWs parameterization used and tested in a well-established AGCM, emphasizing the most recent developments, like the introduction of stochastic techniques and a better specification of the GWs sources. The significance of GWs on the global climate is then illustrated by making sensitivity tests where the frontal and convective GWs parameters are moderatly changed. These changes impact the structure of the jets in the midlatitude stratosphere and the intensity of the sudden stratospheric warmings.

The paper also presents a method to calculate long-range infrasound propagation, and to incorporate the contribution of the GWs that are parameterized in the AGCM. We then show that the changes in GW parameters tested in the model also impact infrasound propagation. This makes infrasound detection a potential tool to tune GWs parameterization in large-scale models.

1 Introduction

The parameterization of gravity waves in climate models is critical for the proper representation of the circulations of both the troposphere and the middle atmosphere in Atmospheric General Circulation models (AGCMs). The orographic gravity waves sig-

nificance is described in the previous issue of this serie [*Lott and Millet*, 2009] whereas it is well established that the non-orographic GWs are responsible for the reversal of the meridional Temperature gradient at the mesopause [*Holton*, 1982] and that they are a substantially driving the quasi-biennal oscillation (QBO) in the equatorial lower stratosphere [*Lindzen and Tsay*, 1975].

In order to parameterize the non-orographic GWs some scheme like *Alexander and Dunkerton* [1999] bin the spectral domain with a large number of monochromatic waves, an approach where the GWs sources can be easily introduced [*Beres et al.*, 2005], but that can be very expensive. Today, to circumvent this difficulty, the spectral domain is sampled by stochastic methods [*Eckermann*, 2011; *Lott et al.*, 2012a; *Lott and Guez*, 2013; *de la Camara and Lott*, 2015], an approach that is further justified by the fact that (i) the mesoscale dynamics producing the GWs is chaotic and (ii) the spread of the ensemble climate predictions need to be increased by stochastic forcings [*Palmer*, 2012].

It is now generally recognized that long-range infrasound propagation is controlled by the stratospheric and mesospheric wind and temperature vertical profiles [*Rind*, 1978; *Gossard and Hooke*, 1975]. During the past ten years extensive simulations were carried out (*Kulichkov et al.* [2010]; *Chunchuzov et al.* [2011]; *Hedlin et al.* [2012]; *Bertin et al.* [2014], among others) confirming that these profiles yield distinct infrasound ducts, which make that a sound emitted at a given source can have several distinct arrivals. In infrasound propagation modeling, the wind and temperature profiles are usually obtained by blending results of weather prediction centers (e.g. ECMWF) with semi-empirical models of winds and Temperature for altitude around 90km and above (upper mesosphere lower thermosphere *Drob et al.* [2008]; *Picone et al.* [2002]). Nevertheless, these datasets only capture variations along quite large horizontal and vertical scales (the so-called "resolved scales"), and using these data, there are systematic missfits between predicted and observed infrasound amplitudes and waveform. One reason can be that when the acoustic ducts are borderline, in the sense that small disturbances can create or destroy a duct, the signal propagation becomes very sensitive to wind fluctuations (e.g. *Bertin et al.* [2014]; *Dergham and Millet* [2013]), which produces highly dispersed signals. In the middle atmosphere the origin of these fluctuations is likely to be due to GWs, and recent works (e.g. *Lalande and Waxler* [2016]; *Hedlin and Drob* [2014]; *Drob et al.* [2013]) show that their main effect is to spread the incoming infrasound signal. Without accounting for GWs, the duration of stratospheric signals is often underestimated, by a factor of 5-10. In such

cases also, deterministic modeling fails in predicting the waveforms and a statistical analysis of sound propagation appears necessary to estimate the uncertainties. A problem with these studies is that in the middle atmosphere, the amplitude and characteristic of the GWs are still not well known. In this context we propose to test GWs field which are consistent with those reducing systematic biases in AGCMs. To specify large-scale winds that are consistent with in-situ infrasound observations, we will nevertheless follow *de la Camara et al.* [2014] and run the scheme off-line using the large scale winds provided by the ECMWF ERAI analisys up to the mesosphere and by an empirical model above.

The purpose of the present paper is to present the research framework we have recently built to improve infrasound calculations and gravity wave parameterizations. To that end, section 2 presents the non-orographic gravity wave scheme recently introduced in the stratospheric version of the LMDz climate model and its impact. To illustrate the significance of the parameterized waves we will make changes in the parameterization set-up and discuss their impacts. In section 3, we briefly expose one of the technique we use to evaluate infrasound propagation from a given source to a given receiver, and take the example of the Hukkakero ammunition destruction done August 18, 2016 at 12:30pm. We then expose how gravity waves fields can be included and show results for the two setups of the GWs parameterization we use.

2 Formalism

The stochastic method introduced in [*Eckermann*, 2011; *Lott et al.*, 2012a] to represent GWs consists in representing the subgrid-scale GWs field by a stochastic Fourier series

$$w' = \sum_{n=1}^{n=\infty} C_n \hat{w}_n(z) e^{z/2H} e^{i(\vec{k}\cdot\vec{x}-\omega t)} \tag{1}$$

where w' is the vertical velocity, z the vertical log-pressure coordinate, $H = 7$km a vertical scale characteristic of the middle atmosphere temperatures, $\hat{w}_n(z)$ the complex vertical structure of a given harmonic, $\vec{k}$ its horizontal wavenumber, ω its absolute frequency, $\vec{x}$ and t being horizontal position and time respectively. In (1) the parameter C_n measures the amplitude of a given harmonic to represent the total wave field (for instance

at a given place inside the model gridbox), it is often referred to as an intermittency coefficient, its statistical interpretation makes that it satisfies

$$\sum_{1}^{\infty} C_n^2 = 1. \tag{2}$$

On top of this statistical decomposition, $\vec{k}$ and ω are also chosen randomly within bounds covering the space and time scales we believe the model does not solve well. To describe vertical propagation, we derive from (1) an EP-flux due to the waves

$$\vec{F}^z = \rho_0(z)\overline{\vec{u}'w'} = \sum_{n=1}^{n=\infty} C_n^2 \vec{F}_n^z \text{ where } \vec{F}_n^z = \rho_r \Re\left\{\frac{\hat{\vec{u}}_n \hat{w}_n^*}{2}\right\}, \tag{3}$$

where $\vec{F}_n(z)$ is the EP-flux carried by each waves, $\rho_0(z) = \rho_r e^{-z/H}$ being a characteristic density vertical profile ρ_r being constant. We then make a WKB evaluation of each harmonics introducing a diffusivity $\nu(z) = \mu/\rho_0(z)$, and limiting each wave amplitude to its statically marginal stability limit. From such consideration and from the Eliasen-Palm theorem, telling that the EP flux is constant for steady linear wave in the absence of dissipation, we construct the vertical profile of $\overline{F}_n^z$ following the iterative rule from one model level (z) to the next above ($z + \delta z$):

$$\begin{aligned}\vec{F}_n^z(z+\delta z) = \frac{\vec{k}\Omega}{|\vec{k}||\Omega|}\Theta\left(\Omega(z+\delta z)\Omega(z)\right) \\ \text{Min}\left\{|\overline{F}_n^z(z)|e^{-2\frac{\mu N^3|\vec{k}|^3}{\rho_0\Omega^4}\delta z}, \rho_r S_c^2 \frac{|\Omega|^3 k^{*2}}{N|\vec{k}|^4}\right\}\end{aligned} \tag{4}$$

where the first fraction guarantees that the EP-flux is in the direction of the phase speed, the second term with Heaviside function $\Theta(z)$ handles critical levels, e.g. places where the intrinsic frequency $\Omega = \omega - \vec{k}\vec{U}$ changes sign ($\vec{U}$ being the background wind), the first term in the parenthesis expresses the decay of the EP flux due to diffusion, and the last term is the saturated EP-flux. Still in (4) N is the buoyancy frequency whereas k^* is the minimum GW wavelength parameterized and S_c is a tunable parameter that controls the wavebreaking.

To relate the gravity waves to their non-orographic sources, e.g. convections and fronts, we then follow *Lott and Guez* [2013] and *de la Camara and Lott* [2015] and represent the subgrid scale precipitation and vorticity by stochastic series,

$$P' = \sum_{n=1}^{\infty} C_n P_n e^{i(\vec{k}\cdot\vec{x}-\omega t)}, \;\; q' = \sum_{n=1}^{\infty} C_n q_n e^{i(\vec{k}\cdot\vec{x}-\omega t)}. \tag{5}$$

In *Lott and Guez* [2013], the precipitation is translated into a heating over a characteristic depth Δz and integrated into a forced Taylor-Goldstein equation solved via a Green function method. It yields a "launched" momentum flux,

$$|\overline{F}^z| = G_0 \rho_r \left(\frac{RL_c}{\rho_r H c_p}\right)^2 \frac{|k|^2 e^{-\frac{N^2|\vec{k}|^2\Delta z_1^2}{\Omega^2}}}{N|\Omega|^3} P^2, \tag{6}$$

where we have assumed that the amplitude of the stochastic projection of subgrid scale precipitation onto the n^{th} harmonics equal the gridscale precipitation P: $|\hat{P}_n| = P$. In (6) the n-indices are dropped for conciseness, R is the dry air gas constant, L_c the latent heat of condensation, Δz_1 scales the depth of convection, and G_0 is a tunable constant of order 1.

In *de la Camara and Lott* [2015] the frontal waves are parameterized by realizing that within fronts, relative vortivity anomalies q' are always substantial, and by using closed formula for spontaneous GWs emission from PV anomalies derived in [*Lott et al.*, 2010, 2012b], e.g. by writing,

$$|\overline{F}^z| = G_1 \frac{\Delta z_2}{4f} \int_0^{\infty} \rho(z') N(z') q'^2 e^{-\pi \frac{N}{U_z}} dz', \tag{7}$$

where Δz_2 is a tuneable depth for the PV anomalies, it is near the gridscale depth δz, f is the Coriolis parameter, U_z is the wind shear and G_1 is a tuneable parameter, again of order 1.

3 Test in LMDz

3.1 Experimental setup

The LMDz version used here is one of the configurations designed for the preparation of the sixth coupled model intercomparison project (CMIP6), an evolution of its CMIP5 version presented in *Hourdin et al.* [2013]. For the middle atmosphere, important differences nevertheless needs to be detailed. First the model now has 80 levels, with a top at 1Pa, and a resolution in the lower stratosphere of $\delta z \approx 1$km near $z = 20$km, increasing smoothly to reach $\delta z \approx 1.4$km near $z = 40$km, then the resolution increases more rapidly it equals $\delta z \approx 6$km at the top and there are only 13 levels in the meso-

sphere. ($50 < z < 80$km). Second, the model has ozone specifications that are derived from observational data, rather than from the LMDz-Reprobus model as in CMIP5. The ozone data used being defined only below 1hPa, we make the O_3 mixing ratio above decreasing rapidly as a function of pressure by using the relation,

$$\chi_{O_3}(P < 1\text{hPa}) = \chi_{0_3}(1\text{hPa})\sqrt{\frac{P}{P(1\text{hPa})}}, \tag{8}$$

which reproduces qualitatively the decay with altitude of the daily Ozone in the mesosphere used in *Hourdin et al.* [2013].

Concerning the parameterization of the non-orographic gravity waves, we choose the wavenumber of the waves randomly using a uniform distribution between $10^{-3} > k > k^* = 2.10^{-5}$. Their intrinsic phase speed is also chosen randomly using a Gaussian distribution with standard deviation $U^* = 50$m/s for the convective waves and $U^* = 30$m/s for the frontal waves. Concerning the non-dimensional parameters we take $G_0 = 0.23$ for the convective waves and $G_1 = 4$ for the frontal waves. Also, the launching altitudes is around $z_l = 500m$ for the frontal waves and $z_l = 5km$ for the convective ones. Finally, we take for the saturation parameter $S_c = 0.6$ and for the diffusion $\nu = 1$. For completeness the subgrid scale orography parameters values are quite different from those given in *Lott and Millet* [2009], see their Eqs $23.1 - 23 - 6$: we now take $H_{NC} = 1.$, $C_d = 0.5$, $G = 0.1$, $\beta = 0.1$, $Ri_c = 1$, and $C_l = 0.5$. Here H_{NC} represents the critical value of the non-dimensional mountain height above which the low level flow is blocked, C_d the drag coefficient applied to the blocked flow, G the gravity wave drag coefficient, β the fraction of the gravity wave drag that propagates freely in and aloft the free troposphere, Ri_c the critical Richardson number controlling orographic gravity waves breaking, and C_l the mountain lift coefficient introduced in *Lott* [1999].

The results presented in this paper are from a 15-yrs experiment where sea surface temperature, sea-ice and ozone are imposed from climatologies constructed with 1979-2008 data. To illustrate how the GWs impact the simulated climate in the middle atmosphere we also show an experiment with slower frontal waves, $U^* = 10$m/s. In this configuration the drags stay reasonable in the middle atmosphere if we take a slightly smaller $G_1 = 2$ and a much larger $S_c = 6.7$. In this setup the frontal wave drag is slightly smaller than in the frst experiment. Conversely, we also increase the convective wave drag constant to $G_0 = 0.6$ in order to increase the convective wave drag.

3.2 Midlatitude Climatologies and sudden stratospheric warmings

The zonal mean zonal winds for January, April, August and October are shown in the 4 panels in Fig. 1a. It shows that the stratospheric winds in the winter midlatitudes are oriented eastward and exhibit well defined jets with maxima centered near 60^0N in the NH and 60^0S in the SH. These are the so called polar night-jets and their maximum value is about right in the NH midlatitude. Still during solstices, the winds are essentially westward in the summer hemisphere, with well define maxima in the subtropical regions above the stratopause. In the mesosphere the winds decay in amplitude as a function of altitude, also consistent with observations, and we know that these decays are only realistic if we have the right amount of gravity wave drag (see *Lott and Millet* [2009]). During equinoxes, the polar jets are eastward in both hemispheres, with amplitudes substantially smaller than the polar night jet during the solstices. In autumn, these easterlies indicate the building up of the winter polar night characterizing the polar vortices, whereas in spring they are associated to their breakdown. The fact that the GW drag control the amplitude of these jets is clearly illustrated in Fig. 1b, which shows that the maximum jets amplitude are everywhere larger when the launched frontal GW drags are reduced.

To characterize the variability of the polar night jets, the Fig. 2a presents the evolution of the 30hPa zonal mean zonal wind at 60^oSouth and North of the 10hPa zonal mean polar temperature at 10hPa. This diagnostics usually characterizes the onset of the so-called sudden stratospheric warmings (SSWs), corresponding to years with polar vortex breakdown, e.g. a time whene the polar jet ceases and even reverses (Fig. 2a and when the winter Temperaure can be 90K above its climatological value, e.g. larger than its summer mean. Again the model winter warmings are quite realistic in the NH, where they are much more pronounced than in the SH. This is of course consistent with observations: SSWs are first related to the breaking of planetary scale Rossby waves, these are much smaller in the SH because there the land-sea contrasts are much less pronounced than in the NH.

The gravity waves also affect the SSW, to a certain extent, and this is partly because they affect the zonal mean flow which controls the index of refraction of the Rossby waves. To illustrate this point Fig. 2b presents the diagnostics of SSWs with reduced frontal GWs. In them we see that the maximum winds attained in winter are almost 10m/s larger

than with larger frontal GW drag. The minimum polar temperature are also typically 10K smaller. The amplitude of the variabilities is also increased accordingly by almost the same amount (i.e. 10K). As a "rule of thumb", we could say that the winter variability, from minimum to maximum goes from the average winter minimum to the averaged summer maximum. As GW drag increases the former, it increases within the same amount the variability.

3.3 Tropics and the quasi-biennal oscillation

In the absence of GWs drag the LMDz model, like any other model, fails in producing a QBO. This is related to the observationnal fact that the large scale equatorial waves alone are not large enough to force the QBO: it is generally admitted that they contribute one half only, the second being the GWs. Therefore, we have tuned the convective GWs scheme in order that the model produces a QBO, and the results are in Fig. 3a. In it we see that the Equatorial winds at the equator alternate positive and negative phase, within a cycle that has a irregular period of almost 26 months. This is a little faster than the observed QBO (e.g., 27-28 months) but the difference can easily be corrected by slightly decreasing the GWs amplitude. Apart from this difference, the model QBO presents the characteristic features of this oscillation, like a decending phase, a relation with the annual cycle at its top near $1hPa$. To illustrate again that the oscillation is very sensitive to the GW drag, Fig. 3b shows the zonal mean wind at the equator when the launched convective GWs stress is increased. In this case, the periods of the oscillation falls to 16monthes, and the amplitude of the oscillation in the low stratosphere is also substantially increased.

4 Impact of GWs on infrasound propagation

4.1 Formalism

The classical approach in infrasound propagation modeling consists in solving the wave equation, often in cylindrical coordinates (r, θ, z), where r and z are the distance from the source and altitude, respectively. While the nature of the source significantly influences the pressure field, a simpler and common way to account for the source is to introduce driving forces on the right-hand side of the wave equation. Hence, using the form of a Dirac delta function $\delta(z - z_0)\delta(r)s(t)$, where $s(t)$ is the source function, the

pressure fluctuation reads as,

$$p(z,r,t) = \frac{1}{2\pi}\int_{-\infty}^{+\infty} \tilde{s}(\omega)\tilde{p}(z;r,\omega)e^{-i\omega t}\mathrm{d}\omega, \tag{9}$$

where $\tilde{s}$ is the Fourier transform of the source. The solution of the homogeneous wave equation is then a solution of the inhomogeneous equation except at height z_0 where the field variables are not generally continuous.

The solution in normal modes (*Jensen et al.* [1994]) of the wave equation can be attacked as two quite distinct problems: (1) finding the eigenpairs in a horizontally homogeneous atmosphere of arbitrary temperature and wind distribution in the vertical direction and (2) synthesis of the waveform at a given range r and time t resulting from a specified source. While the general solution of such problems leads to the so-called leaky modes, open modes (*Budden* [1961]), these modes are usually neglected for infrasound application. Hence, in the normal mode approximation, one seeks the total pressure fluctuation as a sum of M modal contributions;

$$\tilde{p}(r,z;\omega) \approx \sum_{m=1}^{M(\omega)} \frac{\phi_m(0,\omega)\phi_m(z;\omega)}{\sqrt{k_m(\omega)}} e^{ik_m r}, \tag{10}$$

where ϕ_m and k_m satisfy the Helmholtz equation

$$\frac{\partial^2\phi_m}{\partial z^2} + \left[\frac{\omega^2}{c(z)^2} - k_m^2\right]\phi_m = 0, \tag{11}$$

where $c(z)$ is the effective sound speed. Here we use the effective sound speed approximation (*Godin* [2002]), in which the component of the horizontal wind speed in the direction of propagation is added to the thermodynamic sound speed,

$$c(z) = \sqrt{\gamma RT(z)} + \frac{\vec{k}\cdot\vec{u}(z)}{|\vec{k}|} \tag{12}$$

where the index m on the wavevector is dropped because only the projection on the direction of sound propagation matters: $c(z)$ is not a function of m.

At $z = 0$ we use with a Neumann boundary condition and the eigenfunction ϕ_m in (10) is suitably normalized (*Jensen et al.* [1994]). Finally, the signal is obtained by applying the inverse Fourier transform (9), where the integration is performed along a path lying along the real axis. In order to avoid singularities and spurious noncausal effects, the frequency parameter ω is treated as a complex variable $\omega = \omega_r + i\omega_i$ (*Bertin et al.* [2014]), with a small positive imaginary part $\omega_i \ll 1$ and thus, the eigenvalues $k_m(\omega)$ are also complex.

Using the normal mode approach to compute the acoustic pressure field, the impact of GWs is evaluated as follows. Firstly, the large-scale vertical profiles of temperature and winds are extracted from ECMWF products, typically up to 70km. The profiles are matched with the empirical models HWM07 (*Drob et al.* [2008]) and MSIS-90 (Mass Spectrometer and Incoherent Radar Model) through interpolation functions. These two empirical models provide a statistical representation of the mesosphere and thermosphere. The resulting profiles allow computing both the effective sound speed $c(z)$, through the effective sound speed approximation, and the GW field. Secondly, the off-line version of the GW model is used to estimate the impact of GWs onto the vertical profiles. Since the scheme described in section (2) only predicts fluxes $\vec{F}_n^z$ for randomly chosen wavevectors $\vec{k}_n$ and frequencies ω_n, it is necessary to rederive the GW fields by applying local polarization relations and a WKB formalism, yielding,

$$(\vec{u}', T') = \Re\left\{\sum_{n=1}^{N} C_n(\vec{\hat{u}}_n, T_n) e^{z/2H}, e^{i(\vec{k}_n\cdot\vec{x})-\omega_n t)}\right\} \tag{13}$$

where

$$(\vec{\hat{u}}_n, T_n) = \Re\left\{\left(\frac{N}{\Omega_n}\frac{\vec{k}_n}{|\vec{k_n}|}, -i\frac{N^2 H}{R\Omega_n}\right)\hat{w}_n\right\}, \tag{14}$$

and where the vertical profiles of vertical velocity,

$$\hat{w}_n = \sqrt{\frac{2\|\vec{F}_n^z\Omega_n\|}{\rho_r N}}\exp\left(-i\int_0^z \frac{N\|\vec{k}_n\|}{\Omega_n}dz' + i\chi_n\right), \tag{15}$$

where χ_n is a phase that can be chosen randomly. Then, to evaluate wave fields that are consistent with the parameterization presented in section (2), we proceed stochastically and first compute $n = 100$ realizations of vertical profiles choosing $\vec{k}_n$ and ω_n randomly. From this large number of realizations we reconstruct an ensemble of GW fields picking the intermittent factors C_n randomly as well, but conserving the normalization condition (2).

4.2 A case study

We generally refer to the low frequency band of the acoustic spectrum ($2\pi N < \omega < 2\pi$) as infrasound. Man-made sources in this band are limited to large explosions and to sonic booms generated by rockets and aircrafts. Extensive investigations of such sources have been carried out by numerous authors and examples of infrasonic pressure signatures can be found in the literature. For illustration purpose we consider sound prop-

agation of regional distances, and model the source function in (9) by

$$s(t) = \cos(2\pi f_c t)\,\frac{1-\cos(\pi f_c t)}{2}, \tag{16}$$

where $0 < t < 1/f_c$, and $s(t) = 0$ otherwise.

Fig. 4 shows the vertical profiles of effective sound speed as obtained by adding GWs onto the atmospheric specification profided by ECMWF (analysis, 137 levels). Due to large-scale winds, the effective sound speed presents two relative maxima, at the surface and near the stratopause (around 50km), and two relative minima, at the tropopause and the mesopause. These relative extrema define two regions, often called tropospheric and stratospheric ducts, in which $\omega^2/c^2 - k^2$ can be positive and bounded by regions where it can be negative. The efficiency of the stratospheric duct is controlled by the ability of the mesopause to reflect infrasound or, in terms of normal modes, to trigger a large number of normal modes. When including GWs disturbances, an ensemble of effective celerities is produced, replacing T and $\vec{u}$ in Eq. (12) by $T+T'$ and $\vec{u}+\vec{u}'$ respectively. Fig. 4c and Fig. 4a show the standard deviations (gray lines) of the resulting profiles predicted by the non-orographic gravity wave parameterization, as obtained with the two sets of GWs parameters used in Figs. 1a and 1b respectively. As pointed out in section 2 and noticed by numerous authors (e.g. *Lalande and Waxler* [2016]; *Drob et al.* [2013]), the GW field produces substantial variations in the effective sound speed all the way through the middle atmosphere. Whereas the first setup of the parameterization induces substantial variations at the mesopause level, the fluctuations obtained with the second setup are more important in the stratosphere and lower mesosphere.

Results of infrasound propagation simulations obtained with the source function defined by (16) are given in Fig. 5 in the form of space-time diagrams. The normalized Hilbert transform of signals is indicated in colors. The most obvious interpretation of signals in Fig. 5 is that each succeeding arrival is "reflected" from higher in the atmosphere so that its path is longer than preceding arrivals. Fig. 6a shows a typical signal, recorded at the I37NO IMS station in northern Norway on August 18, 2016 and particular realizations of numerically obtained signals. In this case, the source is known to be to associated with a near-surface explosion (with a yield of approximately 20-30 t) at the Hukkakero military range in Finland (*Gibbons et al.* [2015]), located 320km away from I37NO. Such event occurs on consecutive days in August and September and provide a useful data set for the study of infrasound propagation.

The signal in Fig. 6a shows a function of the retarded time $t - r/c_0$ where $c_0 = 356$ m.s^{-1}. The first striking result is that the sound signal arrives for positive retarded time, witnessing that it is dominated by signals that have travelled substantially in the upper atmosphere. The first arrival time is due to the tropospheric duct, and we see that it is quite small in amplitude, whereas the second one is much more substantial and due tos the stratospheric duct. The next three panels below show the signals calculated via the normal mode and for a source of the form given by (16) with $f_c = 0.35$Hz. The second panel from the top gives the infrasound prediction without GWs. It shows that the model predicts well the time of arrival and the duration of the tropospheric response but largely underestimates the amplitude of the stratospheric arrival. In the presence of GWs, the separation between the tropospheric and stratospheric ducts can bee much more permeable, allowing a fraction of the signal to travel easier through the stratospheric duct. This is clearly shown in the next two panels where the green curve show that in the presence of GWs field a stronger second arrival is predicted. Interestingly, it is when the GWs phase speed are smaller in the bottom panel that the stratospheric arrivals duration is larger. It is interesting to recall that in this configuration the GWs modify more the celerity maxima at the stratopause according to the left panel in Fig. 4 than the effective celerity minima at the mesopause (right panel in Fig. 4). Finally, it is important to notice that the increase of the stratospheric arrival when there are more GWs in the stratosphere than in the mesosphere is not the result of one particular GW field. The gray shaded curves show the standard deviation of the signals out of 100 GWs fields built stochastically, and confirm that our infrasound prediction clearly improves when the GWs are more confined to the stratosphere.

5 Perspective

While long-range infrasound propagation modeling is a useful tool in geophysics and nuclear treaty verification, the inherent unpredictability of subgrid-scale atmosphere dynamics results in a poorly constrained propagation medium. The general approach in the infrasound research community is to superimpose a single ad'hoc "frozen" disturbance onto the atmospheric specification, obtained through spectral models and to propagate infrasound in the resulting medium. Such an approach, however, fails in representing the impact of small-scale dynamics which is intrinsically statistical and indeed, direct observations in the lower stratosphere show that the gravity wave field is very in-

termittent, and often dominated by well defined large-amplitude and low-probability wave packets.

In this paper we propose another approach, in which the GW field is described by a stochastic field obtained with a multiwave stochastic parameterization of GWs currently in use in an AGCM. The propagation of infrasound can be obtained at a rather low numerical cost with low-order reduced models (*Bertin et al.* [2014]). Such an approach illustrates how two disciplines can benefit from a mutual interaction. Gravity wave fields can be adapted from the climate models and superimposed onto atmospheric specifications in order to improve infrasound predictions. In turn, the infrasound calculations can be used together with observations to constrain the GW parameterizations. In this paper we only give preliminary results and show that a state-of-the-art GW scheme can yield some improvement in infrasound prediction, provided that the phase speed of GWs is much smaller than that currently in use in AGCMs. As pointed out in this paper the duration of signals remains smaller than that observed. On the other hand, To improve GWs parameterization, one should understand which physical processes could place more low phase speed GWs in the stratosphere To improve infrasound models, one direction could be to consider coupling between modes, especially when GWs fields vary in the horizontal and vertical directions.

Acknowledgments

This work was supported by the European Commission's project ARISE2 (Grant Agreement 653980), the ANR/JPI-Climate/Belmont Forum project GOTHAM (ANR-15-JCLI-0004-01) and the Commissariat à l'Énergie Atomique et aux Énergies Alternatives (CEA).

335 ## References

336 Alexander, M. J., and T. J. Dunkerton (1999), A spectral parameterization of mean-
337 flow forcing due to breaking gravity waves, *J. Atmos. Sci*, *56*(24), 4167–4182.

338 Beres, J. H., R. R. Garcia, B. A. Boville, and F. Sassi (2005), Implementation of
339 a gravity wave source spectrum parameterization dependent on the properties
340 of convection in the whole atmosphere community climate model (waccm), *J.*
341 *Geophys. Res.*, *110*(10), 1–13.

342 Bertin, M., C. Millet, and D. Bouche (2014), A low-order reduced model for the long
343 range propagation of infrasounds in the atmosphere, *J. of the Acoustical Soc. of*
344 *Am.*, *136*(1), 37–52.

345 Budden, K. F. (1961), *The wave-guide mode theory of wave propagation*, Logos Press
346 and Elek Book.

347 Chunchuzov, I. P., S. N. Kulichkov, O. E. Popov, R. Waxler, and J. Assink (2011),
348 Infrasound scattering from atmospheric anisotropic inhomogeneities, *Izv., Atmos.*
349 *and Ocean. Phys.*, *47*(5), 540–557.

350 de la Camara, A., and F. Lott (2015), A parameterization of gravity waves emitted
351 by fronts and jets, *Geophys. Res. Lett.*, *42*, 2071–2078.

352 de la Camara, A., F. Lott, and H. Hertzog (2014), Intermittency in a stochastic
353 parameterization of non-orographic gravity waves, *J. Geophys. Res. Atmos.*, *119*,
354 11,905–11,919.

355 Dergham, G., and C. Millet (2013), Range-dependent propagation modeling of infra-
356 sound in complex atmospheres, *AIAA Paper 2013-3209*.

357 Drob, D. P., et al. (2008), An empirical model of the earth's horizontal wind fields:
358 Hwm07, *Journal of Geophysical Research: Space Physics*, *113*, 2156–2202.

359 Drob, D. P., D. Broutman, M. A. Hedlin, N. W. Winslow, and R. G. Gibson (2013),
360 A method for specifying atmospheric gravity wavefields for long-range infrasound
361 propagation calculations, *J. of Geophysical Research*, *118*(10), 3933–3943.

362 Eckermann, S. D. (2011), Explicitly stochastic parameterization of nonorographic
363 gravity wave drag, *J. Atmos. Sci*, *68*(8), 1749–1765.

364 Gibbons, S. J., et al. (2015), The european arctic: a laboratory for seismoacoustic
365 studies, *Seismmological Research Letters*, *86*(3), 917–928.

Godin, O. A. (2002), An effective quiescent medium for sound propagating through an inhomogeneous moving fluid, *J. Acous. Soc. Am.*, *112*, 1269–1275.

Gossard, E. E., and W. H. Hooke (1975), *Waves in the atmosphere*, Amsterdam: Elsevier Scientific Publishing Company.

Hedlin, M. A., C. D. de Groot-Hedlin, and D. Drob (2012), A study of infrasound propagation using dense seismic network recordings of surface explosions, *Bulletin of the Seismological Society of America*, *102*, 1927–1937.

Hedlin, M. A. H., and D. P. Drob (2014), Statistical characterization of atmospheric gravity waves by seismoacoustic observations, *Journal of Geophysical Research: Atmospheres*, *119*(9), 5345–5363.

Holton, J. R. (1982), The role of gravity wave induced drag and diffusion in the momentum budget of the mesosphere, *J. Atmos. Sci.*, *39*, 791–799.

Hourdin, F., et al. (2013), Impact of the lmdz atmospheric grid configuration on the climate and sensitivity of the ipsl-cm5a coupled model, *Climate Dynamics*, *40*, 2167–2192.

Jensen, F. B., W. A. Kuperman, M. B. Porter, and H. Schmidt (1994), *Computational Ocean Acoustics*, American Institute of Physics.

Kulichkov, S. N., I. P. Chunchuzov, and O. I. Popov (2010), Simulating the influence of an atmospheric fine inhomogeneous structure on long-range propagation of pulsed acoustic signals, *Izv., Atmos. and Ocean. Phys.*, *46*(1), 60–68.

Lalande, J.-M., and R. Waxler (2016), The interaction between infrasonic waves and gravity wave perturbations: Application to observations using UTTR rocket motor fuel elimination events, *Journal of Geophysical Research: Atmospheres*, *121*(10), 5585–5600.

Lindzen, R. S., and C. Y. Tsay (1975), Wave structure of the tropical stratosphere over the marshall island area during 1 april - 1 july 1958, *J. Atmos. Sci*, *32*(10), 2008–2021.

Lott, F. (1999), Alleviation of stationary biases in a gcm through a mountain drag parameterization scheme and a simple representation of mountain lift forces, *Monthly Weather Review*, *127*(5), 788–801.

Lott, F., and L. Guez (2013), A stochastic parameterization of the gravity waves due to convection and its impact on the equatorial stratosphere, *J. Geophys. Res.*, *118*(16).

Lott, F., and C. Millet (2009), *The representation of gravity waves in atmospheric general circulation models (GCMs)*, 685-699 pp., Springer Netherlands.

Lott, F., R. Plougonven, and J. Vanneste (2010), Gravity waves generated by potential vorticity anomalies, *J. Atmos. Sci*, *67*, 157–170.

Lott, F., L. Guez, and P. Maury (2012a), A stochastic parameterization of non-orographic gravity waves: Formalism and impact on the equatorial stratosphere, *Geophys. Res. Lett.*, *39*(6).

Lott, F., R. Plougonven, and J. Vanneste (2012b), Gravity waves generated by sheared three-dimensional potential vorticity anomalies, *J. Atmos. Sci*, *69*(7), 2134–2151.

Palmer, T. N. (2012), Towards the probabilistic earth-system simulator: A vision for the future of climate and weather prediction, *Quart. J. Roy. Meteor. Soc.*, *138*, 841–861.

Picone, J. M., A. Hedlin, D. Drob, and A. Aikin (2002), Nrl msise-00 empirical model of the atmosphere: statistical comparisons and scientific issues, *J. Geophys. Res.*, *107*, doi:10.1029/2002JA009430.

Rind, D. H. (1978), Investigation of the lower thermosphere results of ten years of continuous observations with natural infrasound, *J. of Atmospheric and Solar-Terrestrial Physics*, *40*, 1199–1209.

a) Control values of the GWs drag parameter.

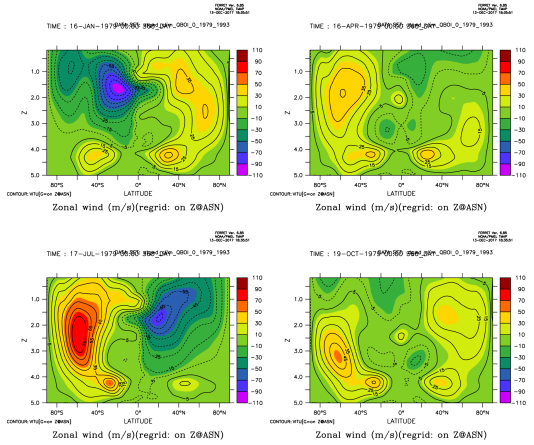

b) Modified values of the GWs drag parameter.

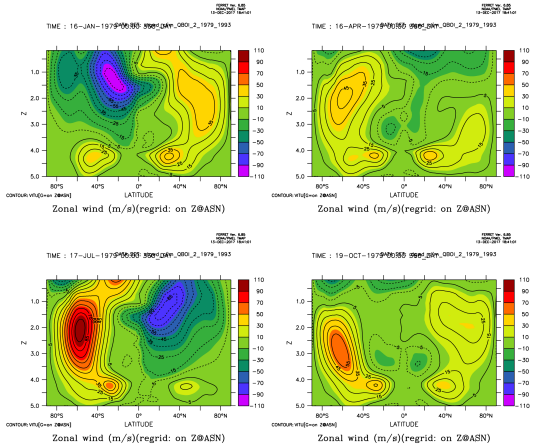

Figure 1. Climatology of the zonal wind in the control and experiments with changed GWs drage parameter.

a) Control values of the GWs drag parameter.

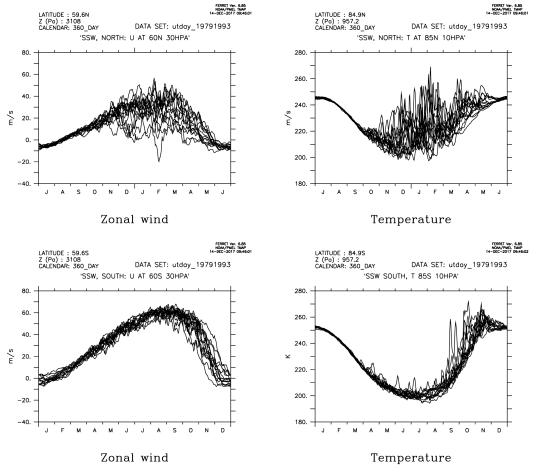

b) Modified values of the GWs drag parameter.

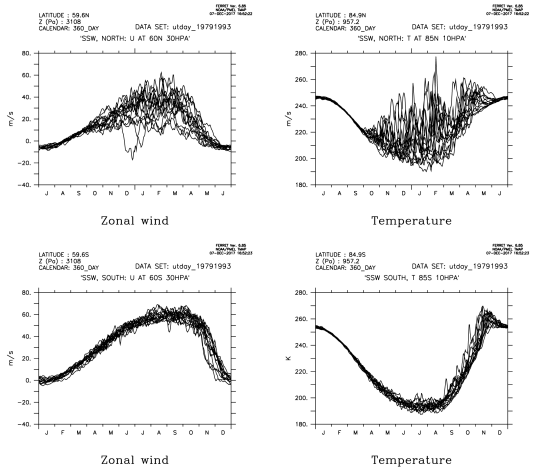

Figure 2. Zonal mean zonal wind at 30hPa (upper left: 60N, upper right: 60S), and polar temperature at 10hPa (upper right: 85N, lower right 85S).

a) Control values of the GWs drag parameter.

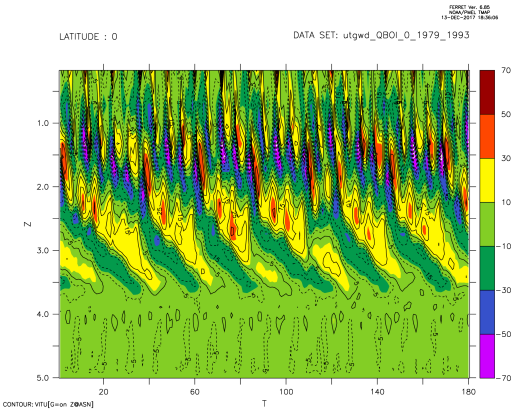

Zonal wind (m/s)(regrid: on Z@ASN)

b) Modified values of the GWs drag parameter.

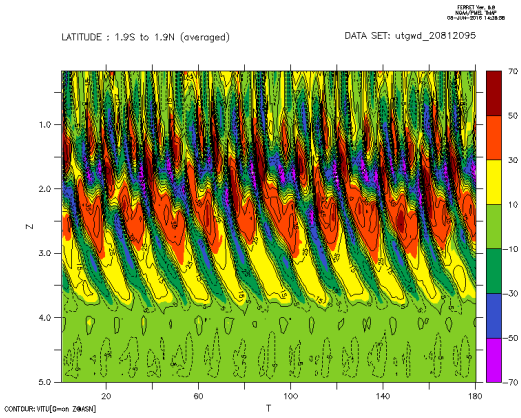

Zonal wind (m/s)(regrid: on Z@ASN)

422 **Figure 3.** Zonal mean zonal wind at Equator.

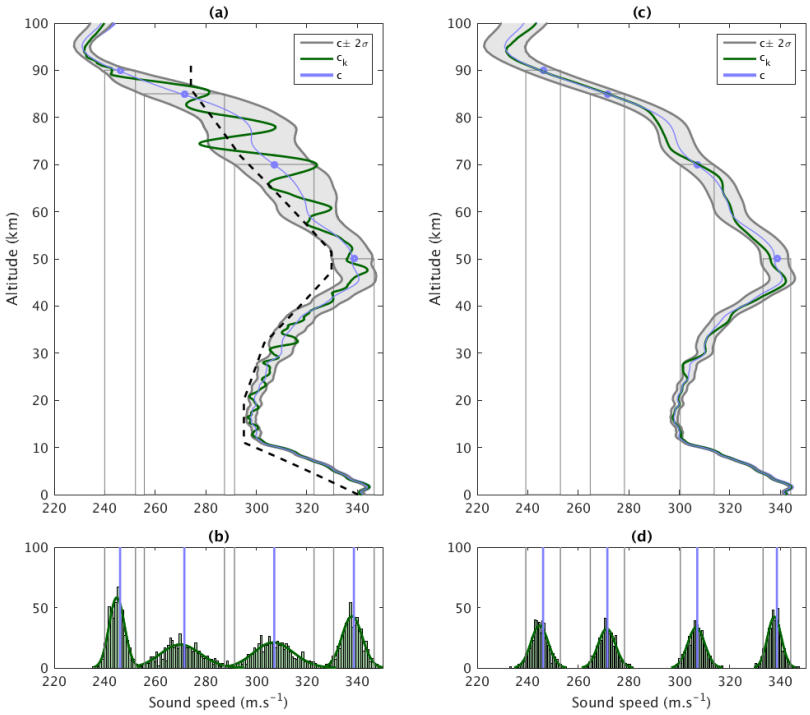

Figure 4. (a,c) Profiles of effective sound speed at I37NO on 16 August, 2016 (12:30pm) and associated probability density functions (b,d) for fixed altitudes of 50, 70, 85 and 90km. The dashed black line gives the profile as obtained from the US76 empirical model. The envelope delimited by gray lines represents the standard deviation $c \pm 2\sigma$ obtained for an ensemble of 500 profiles evaluated stochastically using the setup of Fig. 1 (c,d) and from a parameterization with reduced phase speed waves (a,b). The original reference profile is indicated by $c(z)$ (which is also the mean profile) and a particular realization $c_k(z)$ is given by the green line.

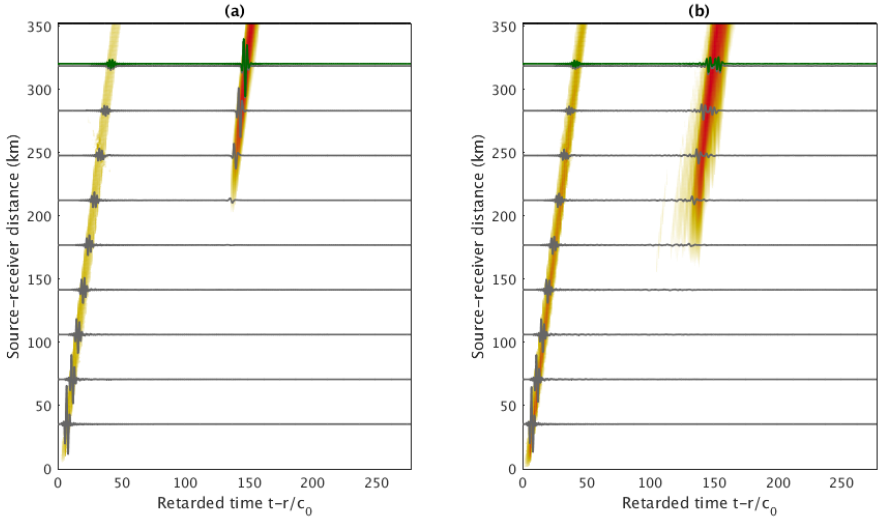

Figure 5. Space-time diagrams showing infrasound signals (green lines) propagating through a particular realization of the perturbed atmospheric specification. The standard deviation of the normalized Hilbert transform of signals is given by colors for an ensemble of 100 vertical profiles. (a) Results obtained using the setup of Fig. 1; (b) results obtained from a parameterization with reduced phase speed waves. The source frequency is $f_c = 0.35$ Hz.

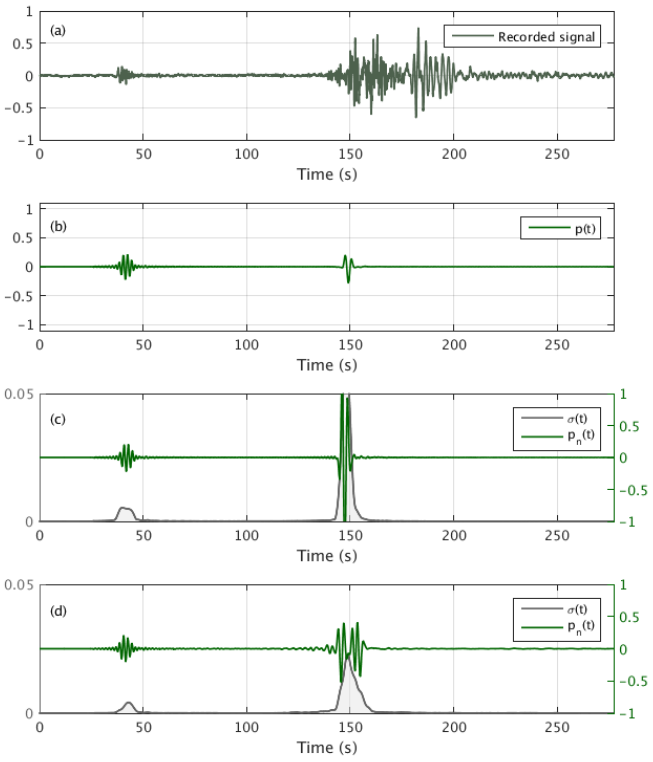

435 **Figure 6.** Recorded signal at I37NO (a) and numerically obtained signals using the 137-levels
436 ECMWF profile (b) and by adding gravity waves. (a) Particular signal obtained using the setup
437 of Fig. 1 and (b) from a parameterization with reduced phase speed waves. Results are obtained
438 for a source function defined by Eq. (16) with $f_c = 0.35$ Hz. The standard deviation σ is plot-
439 ted in solid gray line as a function of time and normalized by the maximum amplitude of each
440 realization.